IVYSPRING INTERNATIONAL PUBLISHER

Theranostics

2018; 8(4): 1168-1179. doi: 10.7150/thno.20271

Research Paper

Diagnosis of LVAD Thrombus using a High-Avidity Fibrin-Specific ^{99m}Tc Probe

Grace Cui[1], Walter J. Akers[2], Michael J. Scott[1], Michael Nassif[1], John S. Allen[1], Anne H. Schmieder[1], Krishna S. Paranandi[1], Akinobu Itoh[3], Dmitry D. Beyder[4], Samuel Achilefu[2], Gregory A. Ewald[1], Gregory M. Lanza[1]✉

1. Division of Cardiology, Washington University School of Medicine, St. Louis, MO
2. Mallinckrodt Institute of Radiology, Washington University School of Medicine, St. Louis, MO
3. Division of Cardiothoracic Surgery, Washington University School of Medicine, St. Louis, MO
4. Barnes-Jewish Hospital, St. Louis, MO

✉ Corresponding author: Gregory M. Lanza, M.D. Ph.D. Division of Cardiology, Campus Box 8215, 660 Euclid Ave, Washington University School of Medicine, St. Louis, MO 63108 Tel: 314-454-8813, Fax: 314-454-5265. Email: greg.lanza@mac.com

Received: 2017.11.05; Accepted: 2017.12.09; Published: 2018.02.02

Abstract

Treatment of advanced heart failure with implantable LVADs is increasing, driven by profound unmet patient need despite potential serious complications: bleeding, infection, and thrombus. The experimental objective was to develop a sensitive imaging approach to assess early thrombus accumulation in LVADs under operational high flow and high shear rates.

Methods: A monomeric bifunctional ligand with a fibrin-specific peptide, a short spacer, and ^{99m}Tc chelating amino acid sequence (F1A) was developed and compared to its tetrameric PEG analogue (F4A).

Results: ^{99m}Tc attenuation by LVAD titanium (1 mm) was 23%. ^{99m}Tc-F1A affinity to fibrin was K_d ~10 μM, whereas, the bound ^{99m}Tc-F4A probe was not displaced by F1A (120,000:1). Human plasma interfered with ^{99m}Tc-F1A binding to fibrin clot ($p<0.05$) in vitro, whereas, ^{99m}Tc-F4A targeting was unaffected. The pharmacokinetic half-life of ^{99m}Tc-F4A was 28% faster (124±41 min) than ^{99m}Tc-F1A (176±26 min) with both being bioeliminated through the urinary system with negligible liver or spleen biodistribution. In mice with carotid thrombus, ^{99m}Tc-F4A binding to the injured carotid was much greater (16.3±3.3 %ID/g, $p=0.01$) than that measured with an irrelevant negative control, ^{99m}Tc-I4A (3.4±1.6 %ID/g). In an LVAD mock flow-loop (1:1, PBS:human plasma:heparin) operating at maximal flow rate, ^{99m}Tc-F4A bound well to phantom clots in 2 min ($p<0.05$), whereas ^{99m}Tc-F1A had negligible targeting. Excised LVADs from patients undergoing pump exchange or heart transplant were rewired, studied in the mock flow loop, and found to have spatially variable fibrin accumulations in the inlet and outlet cannulas and bearings.

Conclusions: ^{99m}Tc-F4A is a high-avidity prototype probe for characterizing thrombus in LVADs that is anticipated to help optimize anticoagulation, reduce thromboembolic events, and minimize pump exchange.

Key words: LVAD, thrombosis, nuclear imaging, fibrin, technetium

Introduction

Heart failure (HF) annually affects over five million Americans of all ages, both sexes, and all races [1]. Patients with refractory Stage D heart failure have limited options: 1) heart transplantation, but only 3,000 donor hearts are available annually; 2) mechanical circulatory support, such as a left ventricular assist device (LVAD); or 3) hospice care with death typically transpiring within months [2-5]. While LVAD placement offers benefits to many patients with severe HF, their successful clinical use requires prevention and management of well-known complications: 1) gastrointestinal bleeding (GIB) due to platelet dysfunction secondary to the high shear effects [6], 2) bacterial infections along the percutaneous driveline, 3) intra-pump thrombus and stroke [7-9]. In terms of hospital readmissions, bleeding, infection, and thrombus were 30%, 22%, and 14%, respectively, in one retrospective study [8].

Prevention of GI bleeding through refinement and shifting of the warfarin International Normalized Ratio (INR) guideline ranges and manipulation of the timing and extent of antiplatelet and anticoagulation regimen used has had anecdotal but no generalized clinical success [10-12]. Multicenter results indicated unexpectedly that lowering the INR range to reduce bleeding events tripled the incidence of pump thrombotic complications [12, 13]. Efforts to manage anticoagulation and minimize bleeding events are complicated by the lack of a sensitive, direct biomarker to characterize LVAD thrombus accumulation or rule it out.

The sensitive and specific diagnosis of pump thrombus remains a clinical dilemma [14-18]. Currently, pump thrombus is suspected based on indirect evidence of increased erythrocyte hemolysis, such as elevated serum lactic dehydrogenase levels (LDH) and decreased serum haptoglobin, changes in LVAD power consumption, or by suggestive echocardiographic signs, such as new aortic valve opening or the lack of left ventricular (LV) decompression with dynamic testing [19]. Echocardiographic ramp studies offer early effective LV optimization of LVAD pump speeds and late pump thrombosis detection in patients suspected of clinical LVAD malfunction [20]. In rare cases, a large pump thrombus may be detected by computed tomography (CT) angiography [21].

Thrombus imaging has a rich history dating back to the mid 1970s and continuing to the present [22]. Both platelets and fibrin have been the dominant thrombus targets studied, but LVAD thrombus is typically an acellular fibrin accretion [23]. Acute vascular thrombi are readily imaged with virtually all clot-specific contrast agents, but aged thrombi greater than 48 h to 72 h are poorly targeted [22]. Thrombus homing is further degraded by anti-coagulation use, which may be clinically necessitated to prevent or treat suspected thrombosis [22]. LVAD thrombus develops over time despite concurrent anticoagulation with warfarin and aspirin [24, 25].

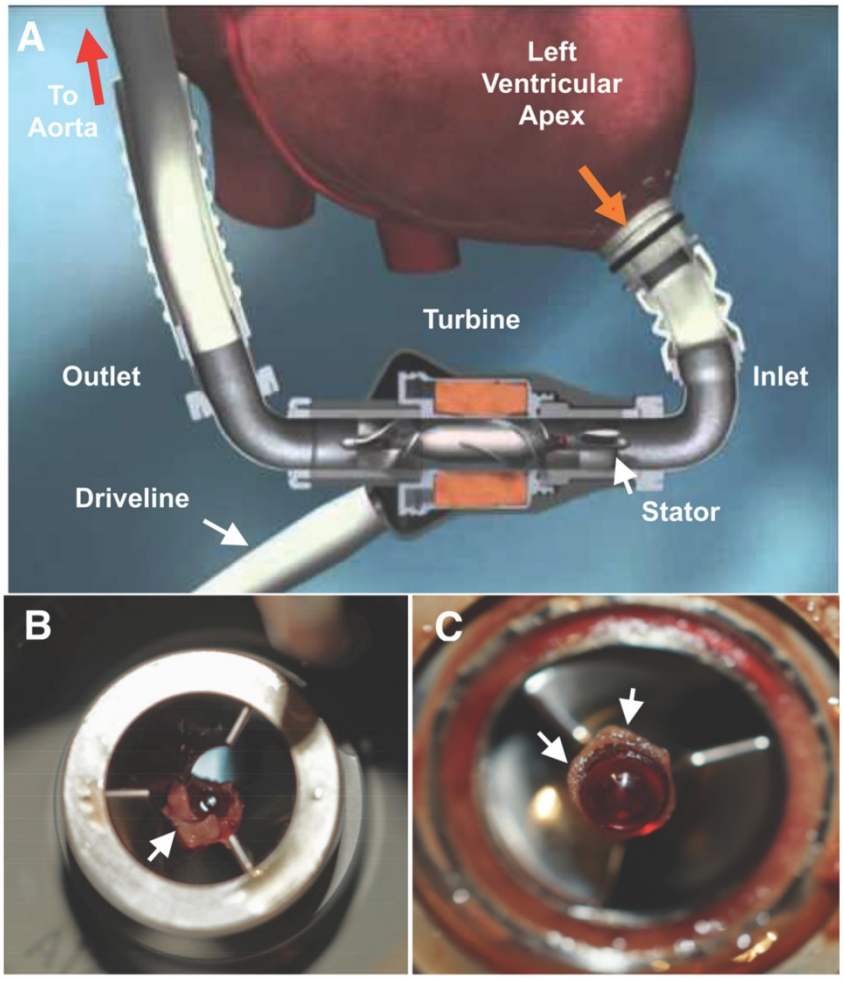

Figure 1. A Diagrammatic representation of a HeartMate II (HMII) left ventricular assist device (LVAD). Blood (orange arrow) is drawn into the pump through a cannula from the ventricular apex, flows by the stator through the turbine and returns to systemic circulation through the outlet cannula into the aorta. The pump is powered through an externalized driveline cable on the outlet side of the LVAD. **B** Small residual LVAD thrombus on the inlet stator and around the bearing (**C**) from a patient admitted with elevated lactate dehydrogenase (LDH) (1300's) after symptomatic hemorrhagic/embolic stroke due to a suspected pump thrombus. White arrows point to residual thrombus. HMII image is copyright protected by Thoratec, Inc and used with permission.

Direct diagnosis and quantification of pump thrombus with noninvasive imaging is further complicated by the LVAD titanium housing, which precludes the use of magnetic resonance imaging (MRI), CT, or ultrasound and favors a nuclear medicine approach. Indeed, the high-shear and high blood flow conditions created by an LVAD, such as the HeartMate II (HMII, Abbott-Thoratec, Lake Bluff, Illinois), spinning at 8,800-10,000 RPM, necessitate a probe with high molecular specificity and extreme binding avidity. Further, radioactive background in blood passing through the pump or accumulating in surrounding organs must be minimized to afford effective signal-to-noise.

The objective of this project was to evaluate a sensitive and specific anti-fibrin probe prototype concept for targeting thrombus in the anticoagulated high-flow, high shear environment of LVADs. Monomeric and tetrameric ^{99m}Tc probes were

evaluated and compared in vitro for fibrin clot binding signal in PBS, with and without a strong amino acid tridentate ligand (cysteine), and plasma. Pharmacokinetic and biodistribution studies of the monomeric and tetrameric nuclear probes were delineated along with selective in vivo targeting to carotid thrombus in mice. The relative binding of the monomeric and tetrameric probes to acute fibrin clots were compared within a Heartmate II mock loop flowing heparinized plasma:PBS at approximately 6 L/min. ^{99m}Tc attenuation through titanium, as used in the pump housing, was characterized. LVADs excised from patients undergoing heart transplant or LVAD exchange were rewired and exposed to the tetrameric fibrin probe in the mock flow-loop system under near maximal flow conditions followed by high-resolution NanoSPECT imaging assessments to assess inherent accumulation of intra-pump thrombus. The overarching result of this proof-of-concept study suggests that direct imaging assessments of LVAD thrombus accumulation, or lack thereof, could improve and individualize patient management decisions with the potential to minimize thrombotic events, decrease hemorrhaging, and reduce surgical pump exchanges.

Materials and Methods

Solid phase synthesis of monomeric (F1A) and tetrameric (F4A) fibrin probes

Monomeric unit (F1A) is a bifunctional entity comprising a fibrin-specific natural peptide analogue (QIWCLGYPCEWQ) [26] interconnected through a diethylene glycol (DEG) spacer to a technetium-chelating amino acid sequence (HHE-DEG) (Figure 2A). PEG_{2000} tetramer was used to couple four F1A monomers to form F4A (Figure 2B). Briefly, peptide precursors were synthesized with a CS136 peptide synthesizer at a 0.2 mmol scale. Standard solid phase Fmoc peptide synthesis was used [27]. F1A was synthesized with high purity (>95%). The final product was analyzed by HPLC and ESI-TOF mass spectrometry: ESI-TOF (positive mode): m/z $[C_{94}H_{126}N_{24}O_{26}S_2 + 2H]^+$ Calcd. 1036.4 Da.; Obsd. 1036.3 Da. To obtain the tetramer, the side-chain protecting group, 4-{N-[1-(4,4-dimethyl-2,6-dioxocyclohexylidene)-3-methylbutyl]-amino}benzyl (Dmab) was selectively removed from glutamate and coupled with the 4-arm-PEG amine (PSB-431, 2K, Creative PEGWorks, Chapel Hill, NC). F4A was purified with size exclusion chromatography (Zeba Desalt Spin Column, 2 mL, ThermoScientific) using 10% acetic acid in water followed by three deionized water washes. The overall yield of F4A was <10%. MALDI characterization of the product revealed an array of molecular weights arising from an unexpectedly high polydispersity of the tetrameric PEG core. (See Supplementary Material).

^{99m}Tc labeling of F1A and F4A

F1A and F4A were radiolabeled to the HHE sequence with ^{99m}Tc for gamma imaging [28]. This was accomplished by adding $Na^{99m}TcO_4$ (~9 mCi; 1.0 mL) in saline to an IsoLink vial (Center for Radiopharmaceutical Sciences of PSI, ETH and USZ, Paul Scherrer Institute, Switzerland). ^{99m}Tc-F1A optimally binds one ^{99m}Tc nuclide and the ^{99m}Tc-F4A chelates up to four metal atoms, one on each arm (Figure 2B). Given the rapid radioactive decay of ^{99m}Tc to ^{99}Tc as well as the elution status of the molybdenum generator yield, typical specific activities of the ^{99m}Tc-F1A and ^{99m}Tc-F4A probes were 40 mCi/μmol with 90% to 95% radiochemical purity based on radio-thin layer chromatography (0.1 M NaAc pH 5.18:MeOH:H_2O = 20:100:200).

Acellular fibrin clot assays

Acellular fibrin clots were used: 1) to characterize the binding affinity of ^{99m}Tc-F1A and the relative avidity of ^{99m}Tc-F4A, 2) to assess the stability of ^{99m}Tc chelation, and 3) to evaluate the matrix effect of plasma on the probe binding to fibrin clots. Uniform clots were produced by quickly admixing 100 μL of fresh frozen human plasma with 3 U thrombin and calcium chloride (Sigma-Aldrich Chemical, St. Louis, MO). The mixture was pipetted into uniform cylindrical plastic tubes. Once formed, clots were washed repeatedly in 0.1 M PBS buffer (pH 7.0) then stored at 4 °C in same until use.

Fibrin binding affinity

^{99m}Tc-F1A (20 μCi) was incubated with the clot samples at 37 °C for 30 min with 1, 5, 10, 15, 25, and 30 μg cold monomer supplemented with 0.1 M PBS pH 7.4 to bring each test volume total to 0.5 mL. The fibrin clots were separated from unbound radioactivity by repeated centrifugation and washing then were counted in a calibrated well counter (Wizard 3, Perkin Elmer, Waltham, MA). Results, adjusted for decay, were used to estimate the dissociation constant (K_d) using the Hill slope model (h), $Y=Bmax*X^h/(Kd^h + X^h)$ (MatLab, Natick, MA) where Kd is the ligand concentration that binds to half the receptor sites at equilibrium, Bmax is the maximum number of binding sites, X is the radioligand concentration and h is the Hill slope, an estimate of binding cooperativity. Total fibrin concentration was estimated from plasma fibrinogen to be 0.735 nmol per clot. ^{99m}Tc-F4A (20 μCi) was incubated with the

clot samples at 37 °C in the presence of unlabeled F1A, which was titrated to a 120,000:1 excess relative to ^{99m}Tc-F4A, to assess the relative avidity of the tetrameric probe.

Assessment of ^{99m}Tc-F1A and ^{99m}Tc-F4A radiolabel stability and plasma interference

Radiolabeled F1A and F4A were bound to clots in the presence of marked excess cysteine to evaluate the stability of the ^{99m}Tc label in triplicate [29]. ^{99m}Tc-F1A or ^{99m}Tc-F4A (20 μCi) supplemented with 0.1 M PBS pH 7.4 (total volume of 0.5 mL) were incubated with fibrin clot samples at 37 °C for 30 min.

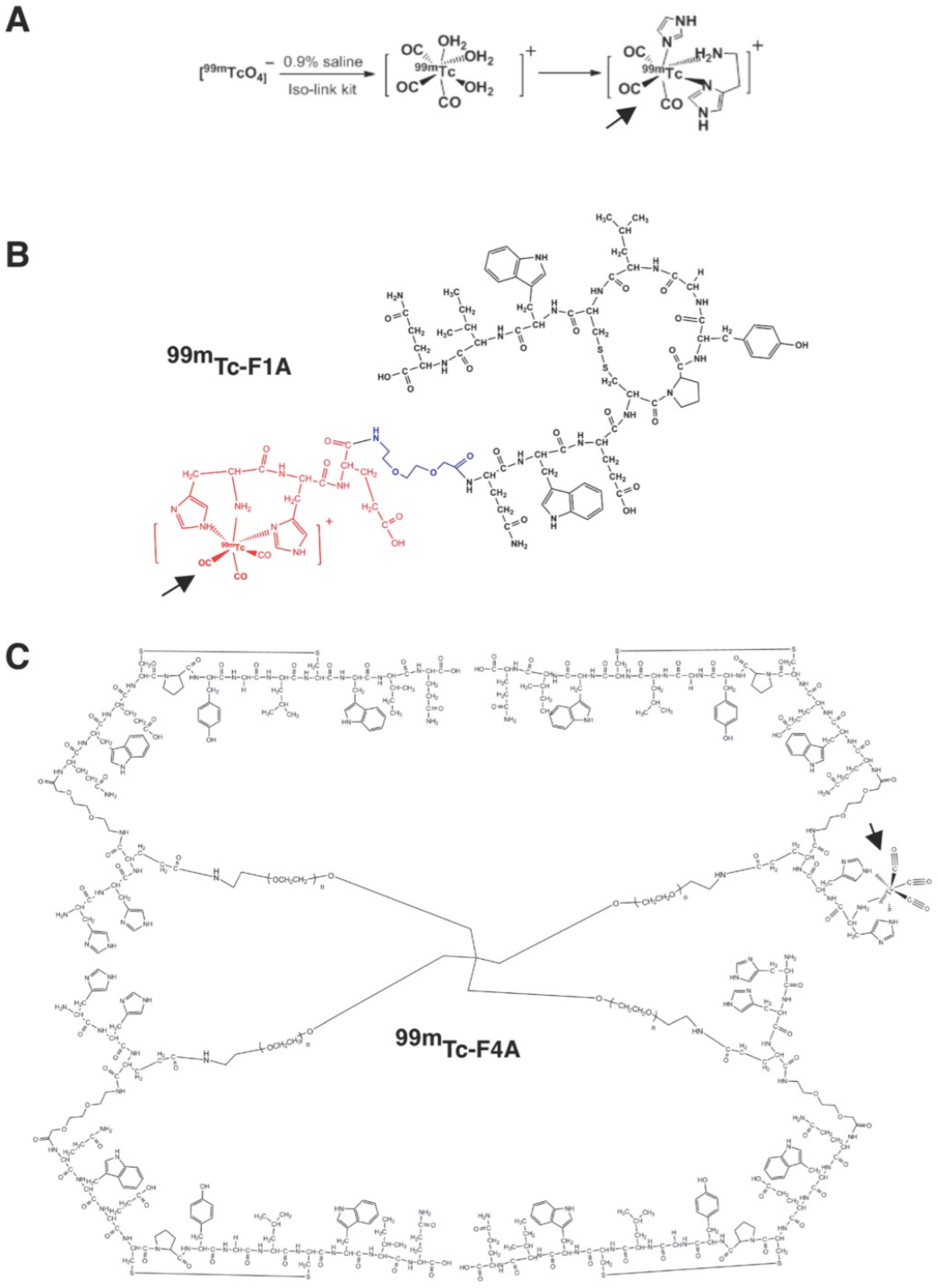

Figure 2. A ^{99m}Tc carbonyl aqua-ion and the complex formed with HH-peptide. **B** ^{99m}Tc-F1A bi-functional monomer depicting the cyclic homing sequence, short spacer, and ^{99m}Tc-chelating site depicting ^{99m}Tc carbonyl coupling. **C** ^{99m}Tc-F4A tetramer created by the balanced cross-linking of the four F1A monomers with tetrameric PEG arms (shown with one example of ^{99m}Tc on one of the four arms for clarity). PEG: polyethylene glycol. Bold arrows point to ^{99m}Tc carbonyl coupling in example illustrations.

Similarly, the 0.1 M PBS buffer diluted 50% with fresh frozen human plasma (total volume of 0.5 mL) was used to assess potential plasma matrix interference on radiolabeled peptide binding in triplicate. In both instances, fibrin clots were separated from unbound radioactivity by repeated centrifugation, were washed, then counted in a calibrated well counter (Wizard 3, Perkin-Elmer).

Gamma signal attenuation from titanium LVAD housing

$Na^{99m}TcO_4$ was serially diluted into plastic snap-cap vials from 20 µCi to 0.5 µCi and radioactivity was evaluated using the Multispectral FX multimodal imaging system (Bruker-Biospin, Billerica, MA) with the isotope phosphor screen for planar scintigraphy using a 1.0 min acquisition time. Samples were imaged before and after placement of a 1 mm titanium sheet provided by Thoratec Corp., which corresponded to the titanium metal used to form the LVAD HMII housing.

Pharmacokinetics (PK) and biodistribution (BD) of ^{99m}Tc-F1A and ^{99m}Tc-F4A in mice

All animal research was conducted under a protocol approved by the Washington University Animal Studies Committee.

The pharmacokinetics of ^{99m}Tc-F1A and ^{99m}Tc-F4A were studied in triplicate in mice (male, Harlan, C57BL/6, 4-6 wks). Mice were anesthetized with ketamine (85 mg/kg) / xylazine (10 mg/kg) and maintained with 1-2% isoflurane through a nosecone. ^{99m}Tc-F1A or ^{99m}Tc-F4A (16-30 µCi) were injected via tail vein and serial blood samples were obtained at 0, 2, 5, 10, 15, 20, 30, 60, 120, and 180 min via an indwelling jugular catheter. Blood samples were timed, weighed, and counted with a calibrated gamma counter (Wizard 3, Perkin-Elmer). The data were adjusted for decay relative to the time of counting and were fit to bi-exponential models using MatLab (Natick, MA). After 180 min animals were euthanized; tissue and fluid aliquots (bladder, brain, GI, heart, lung, liver, spleen, urine, body remains) were excised, weighed, counted, and the results adjusted for decay relative to the time of counting. Biodistribution and pharmacokinetic results were expressed as percent of actual injected dose per gram tissue or fluid (%ID/g).

Efficacy of ^{99m}Tc-F4A in mice with carotid thrombus

In vivo targeting of ^{99m}Tc-F4A was performed in mice (male, Harlan, C57BL/6, 4-6 wks) following the introduction of a carotid thrombus using the Rose Bengal method. [30, 31] Briefly, mice were administered 60 µg/g body weight by tail vein injection of a 20 mg/mL solution of Rose Bengal dye (the singlet oxygen was generated by the photoactivation of the dye). HeNe laser (540 nm, 1.5 mW/cm^2) was focused for 45 min to 50 min on a surgically exposed carotid artery distal to a Doppler cuff probe until blood flow was decreased at least 70% relative to baseline. After laser treatment, the mice were heparinized and ^{99m}Tc-F4A (n=4) or an irrelevant peptide (GGSHPSRPRAG) tetrameric ^{99m}Tc-control (^{99m}Tc-I4A, n=4, 3 µCi/g BW, ~75 µCi/mouse). At 2 h, %ID/g of the thrombotic carotid and its contralateral control vessel were determined using an automatic well counter (Wizard 3, Perkin-Elmer). To confirm in vivo imaging efficacy, an additional secondary cohort of 5 mice with carotid thrombus created as above were administered 40 mCi of ^{99m}Tc-F4A and imaged two hours later with a Multispectral FX multimodal imaging system (Bruker-Biospin, Billerica, MA) with the isotope phosphor screen for planar scintigraphy using a 1.0 min acquisition time.

Fibrin targeting in an LVAD mock flow loop

A HMII LVAD controlled by a computer console was inserted into a 200 mL mock flow loop comprised of ½" plastic tubing interconnecting a PBS:fresh heparinized human plasma (1:1) reservoir, an injection port, a media drainage port, and an inline ½" plastic chamber. Uniform human fibrin clots aged 24 h were supported within the inline chamber using a highly porous, single thread layer of cotton gauze. The LVAD was operated at maximum flow rate (~10,000 RPM, 6 L/flow per minute). ^{99m}Tc-F4A or ^{99m}Tc-F1A (0.5 mCi) were injected into the loop and allowed to circulate for 2 min followed by a 2 min plasma/PBS wash to remove unbound radioactivity. Recovered clot radioactivity was counted in a calibrated gamma well counter and the results adjusted for decay.

Targeting of thrombus in excised LVADs using a mock flow loop

HMII excised (n=5) from patients without clinical suspicion of pump thrombus were rewired for operation in the heparinized human plasma:PBS (1:1) mock loop and operated at the preprogrammed patient controller pump rate of (9400 RPM). ^{99m}Tc-F4A (0.5 mCi) was injected into the loop for 30 min then washed with fresh circulating plasma/PBS for 2 min. The pumps were removed from the loop and imaged with single-photon emission computed tomography (SPECT) with CT (NanoSPECT/CT, Bioscan, Inc., Poway, CA). Helical SPECT and CT scans were performed with 8 projections per rotation for 5 min per projection and 65 kVp, 177 µAs, respectively, and

reconstructed with Invivoscope software. Total photon counts were calibrated to total radioactivity of the sample.

Statistical Analysis

Data were analyzed using Student's T-Tests, paired T-tests, or analysis of variance (SAS Inc., Cary, NC). Data are presented as the mean ± standard error of the mean unless otherwise stated. In vivo targeting of carotid thrombus was a completely randomized design replicated to allow detection of a 20% difference with 80% power at an alpha level of 0.05.

Results

^{99m}Tc-F1A and ^{99m}Tc-F4A fibrin affinity, radiolabel stability, plasma interference

The binding affinity, radio-stability, and plasma matrix effects of the ^{99m}Tc-F1A and ^{99m}Tc-F4A probes were characterized. Titrated dosages of ^{99m}Tc-F1A bound to uniform fibrin clots in PBS with good affinity (K_d ~10.2 μM), which was consistent with the earlier report and phage display-derived peptides in general [26] (Figure 3A). By comparison, ^{99m}Tc-F4A bound with extraordinary affinity and avidity to analogous fibrin targets in PBS. ^{99m}Tc-F4A bound to each clot was not displaced by unlabeled F1A titrated to 120,000 molar excess relative to ^{99m}Tc-F4A, reflecting extraordinary avidity (Figure 3B).

Radiolabel stability of ^{99m}Tc-F1A and ^{99m}Tc-F4A probes was studied in the presence of excess cysteine, a strong tridentate ligand. Fibrin clot nuclear signal measured for ^{99m}Tc-F1A or ^{99m}Tc-F4A binding in PBS with or without cysteine did not differ ($p>0.05$) (Figure 3C, D). However, the binding of ^{99m}Tc-F1A to fibrin clots in the presence of human plasma was severely compromised ($p<0.05$) compared with PBS

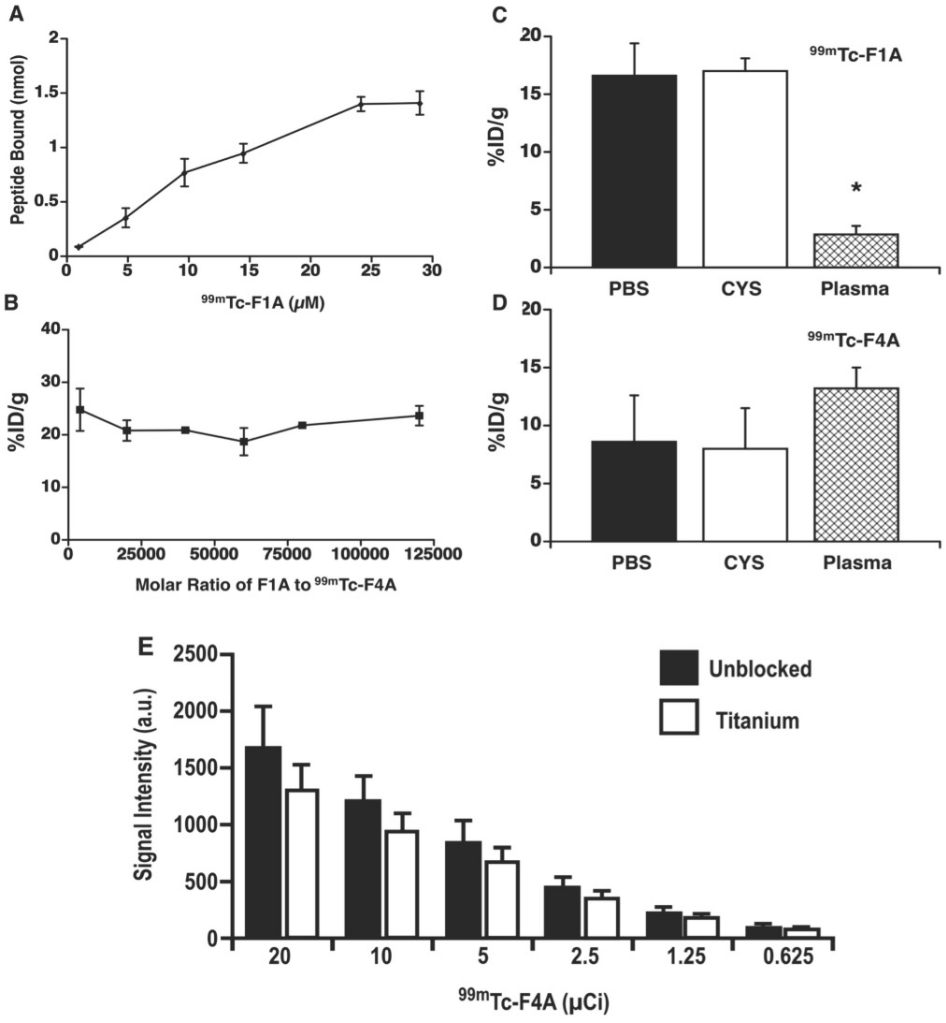

Figure 3. A Titrated dosages of ^{99m}Tc-F1A bound to uniform fibrin clot in PBS. The dissociation constant (K_d ~10.2 μM) was adjusted for decay and estimated using the Hill slope model, $Y=Bmax*X^h / (Kd^h + X^h)$ three times independently (± s.e.m.). Total fibrin concentration was estimated from plasma fibrinogen (0.735 nmol per clot). **B** The percentage of ^{99m}Tc-F4A bound to each clot in the presence of unlabeled F1A (monomer) at molar ratios up to 120,000 to 1. ^{99m}Tc-F1A (**C**) and ^{99m}Tc-F4A (**D**) bound to clots in the presence of PBS and in PBS with excess cysteine to demonstrate ^{99m}Tc labelling stability. However, in a 50:50 PBS:human plasma mixture the binding of ^{99m}Tc-F1A to clot was dramatically reduced ($p<0.05$) whereas ^{99m}Tc-F4A was unaffected. **E** The attenuation of $Na^{99m}TcO_4$ from 20 μCi down to 0.5 μCi by titanium plate (1 mm), equivalent to the housing of HMII, was 23% ± 3% independent of radioactivity level (n=3/level). HMII: HeartMate II; PBS: phosphate buffered saline.

alone, indicating a significant matrix effect (Figure 3C). In contradistinction, ^{99m}Tc-F4A binding was unaffected by human plasma: the probe bound equivalently to the fibrin clots in PBS and in plasma ($p>0.05$) (Figure 3D). Of note, a slight increase in ^{99m}Tc-F4A fibrin signal was appreciated in the presence of plasma, which may reflect blockage of nonspecific binding sites on the plastic well walls, increasing the bioavailability of the free ^{99m}Tc-F4A probe to interact with the clots.

Nuclear signal attenuation due to titanium LVAD housing

The decision to approach the LVAD thrombus diagnosis problem with a nuclear medicine solution reflected the need for the probe signal to penetrate through the titanium pump housing. The attenuation of $Na^{99m}TcO_4$ by a titanium plate of equivalent quality and thickness (1 mm) to that used to form the housing for HMII was evaluated by titrating the isotope concentration from 20 µCi down to 0.5 µCi. Gamma scintigraphy imaging of the phantoms with and without the titanium sheet shielding revealed 23% ± 3% nuclear signal attenuation independent of the level of radioactivity studied (Figure 3E). The influence of signal attenuation due to the titanium housing, although present, was relatively minor, permitting both the high sensitivity and quantitative gamma imaging.

Pharmacokinetics (PK) and biodistribution (BD) of ^{99m}Tc-F1A and ^{99m}Tc-F4A in mice

The pharmacokinetics (PK) and biodistribution (BD) of the reference radiolabeled ^{99m}Tc-F1A were compared to that of the ^{99m}Tc-F4A in mice in triplicate. Both agents closely followed a two-compartment bi-exponential PK model (Figure 4A, B). The alpha distribution half-life of ^{99m}Tc-F4A in mice (5.0 ± 1.9 min) was 41% faster ($p<0.05$) than that of ^{99m}Tc-F1A (8.6 ± 1.9 min). Similarly, the beta elimination half-life of ^{99m}Tc-F4A (124.7 ± 41.3 min) was 50 min shorter (28%) than ^{99m}Tc-F1A (174.2 ± 26.2 min) ($p= 0.08$), which was likely related to the minimal plasma interactions with ^{99m}Tc-F4A.

The organ biodistribution of both agents at the conclusion of the PK study (180 min) was very similar with neither probe accumulating substantially in the lung, liver or spleen. Such low uptake by reticuloendothelial organs reflects the relatively small sizes of ^{99m}Tc-F1A and ^{99m}Tc-F4A. Essentially, all of the ^{99m}Tc activity was excreted through the urinary system into kidney, bladder or urine at the 3 h sampling time point (Figure 4C, D). These data suggest that background circulating ^{99m}Tc-F4A blood pool levels will decrease rapidly without significant tissue accumulation, minimizing the time between probe injection and signal readout.

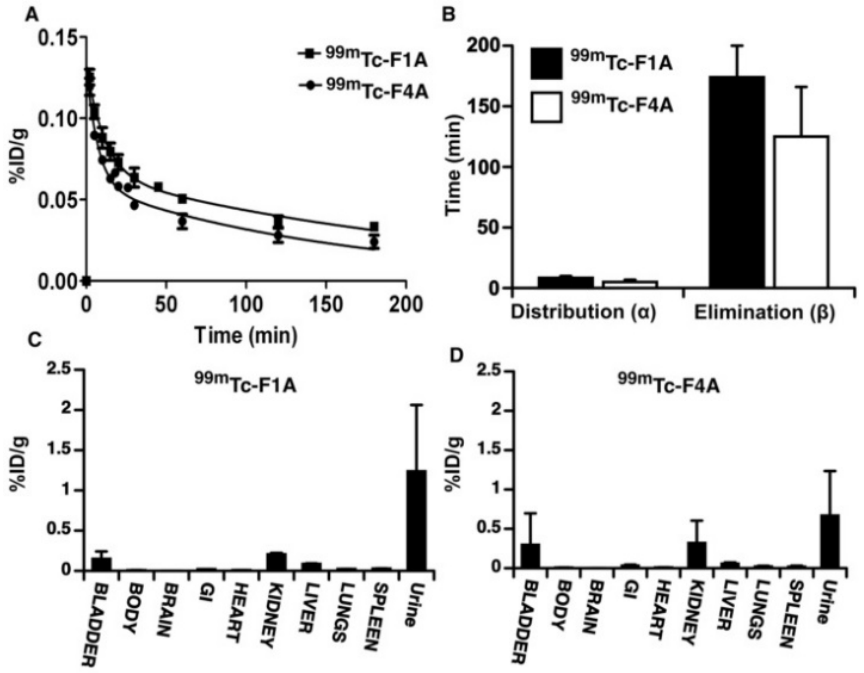

Figure 4. The pharmacokinetics (PK) and biodistribution (BD) of the reference radiolabeled ^{99m}Tc-F1A compared to ^{99m}Tc-F4A in mice (n=3/treatment). **A** Both agents, presented as percent injected radioactivity per gram blood (%ID/g), closely followed a two-compartment bi-exponential PK model. **B** The alpha distribution half-life of ^{99m}Tc-F4A in mice (5.0 ± 1.9 min) was 41% faster (p=0.04) than that of ^{99m}Tc-F1A (8.6 ± 1.9 min). Similarly, the beta elimination half-life of ^{99m}Tc-F4A (124.7 ± 41.3 min) was 50 min shorter (28%) than that of ^{99m}Tc-F1A (174.2 ± 26.2 min) (p= 0.08), which were likely related to minimal plasma interactions with ^{99m}Tc-F4A. Mouse organ biodistribution including body remains (n=3/treatment) of ^{99m}Tc-F1A (**C**) and ^{99m}Tc-F4A (**D**) at the conclusion of the PK study (180 min) were similar. Neither probe accumulated substantially in the lung, liver or spleen. Virtually all of the ^{99m}Tc activity was excreted through the urinary system (kidney, bladder and urine).

Efficacy of ^{99m}Tc-F4A in mice

The targeted binding of ^{99m}Tc-F4A to carotid thrombus was robust and occurred in every animal studied: carotid clot, 16.3 ± 3.3 %ID/g versus contralateral carotid (no clot), 3.1 ± 1.5 %ID/g, $p<0.05$ (Figure 5). ^{99m}Tc-I4A had poor carotid clot binding: carotid clot, 3.4 ± 1.6 %ID/g versus the contralateral clot-free carotid, 1.1 ± 0.5 %ID/g, $p<0.05$. As expected, ^{99m}Tc-F4A (16.3 ± 3.3 %ID/g) binding to the injured carotid was much greater ($p<0.05$) than that measured with ^{99m}Tc-I4A (3.4 ± 1.6 % ID/g). These data corroborate that ^{99m}Tc-F4A effectively, specifically, and systemically targeted native carotid thrombus in vivo.

In a separate cohort of mice bearing carotid thrombus, ^{99m}Tc-F4A was administered by tail vein injection and mice were imaged using Multispectral FX multimodal

imaging system (Bruker-Biospin, Billerica, MA) after 2 h. Figure 5B provides a representative in vivo image showing robust signal (arbitrary units) in the targeted carotid with negligible contrast in the uninjured contralateral vessel. These data suggest that the binding to carotid thrombus occurs relatively soon after injection of ^{99m}Tc-F4A, resulting in strong contrast greater than the circulating background and the contralateral artery at 2 h.

Ex vivo LVAD flow study using a mock loop

The high shear and high blood flow (~6 L/min) of the LVAD required to pump the entire circulating blood volume of the patient every minute place severe demands on probe binding affinity and clot retention of the nuclear probe. Therefore, fibrin clot accumulation of the reference probe, ^{99m}Tc-F1A, and ^{99m}Tc-F4A were compared in triplicate under the maximal flow and shear conditions produced by a HMII using a mock loop circulating a plasma:PBS:heparin mixture (Figure 6B). After 2 min of circulation, ^{99m}Tc-F4A was rapidly bound and retained on the clot whereas the monomeric reference, ^{99m}Tc-F1A, was associated at only negligible levels ($p<0.01$) (Figure 6A). The superior binding of ^{99m}Tc-F4A to fibrin clots under high flow conditions illustrated the advantage of the high avidity PEG-based tetrameric design for increasing fibrin binding and minimizing nonspecific plasma interference.

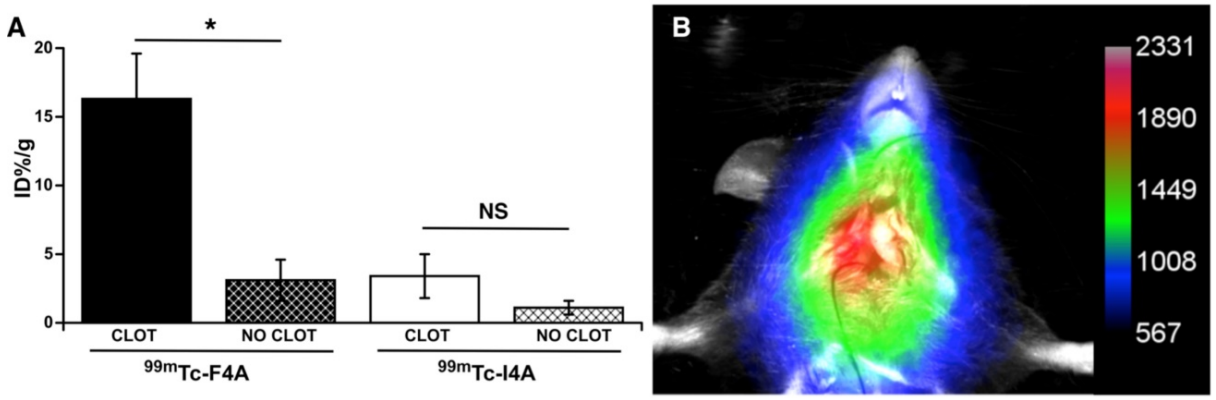

Figure 5. Targeted fibrin binding of ^{99m}Tc-F4A to carotid thrombus was compared to an irrelevantly targeted ^{99m}Tc-I4A probe (~75 μCi/animal). **A** The signal from the clot-bearing carotid (%ID/g) was compared to the clot-free contralateral vessel response. ^{99m}Tc-F4A binding to carotid thrombus was much greater than uptake in the clot-free contralateral carotid vessel ($p<0.05$). ^{99m}Tc-I4A bound poorly to carotid thrombus and nuclear probe uptake did not differ from the nonspecific signal obtained in the clot-free carotid. Binding of the fibrin-specific ^{99m}Tc-F4A to carotid clot was markedly greater ($p=0.01$) than the nonspecific binding of ^{99m}Tc-I4A to thrombus. *$p<0.05$. **B** Representative maximum intensity projection image with a color map (arbitrary units) from 1 of 5 mice administered ^{99m}Tc-F4A (40 μCi) by tail vein injection then imaged 2 h later with a Multispectral FX multimodal imaging system (Bruker-Biospin, Billerica, MA). A Marked single source signal originating from the right carotid thrombus was noted. All animals (n=5) displayed a strong in vivo carotid nuclear signal following ^{99m}Tc-F4A.

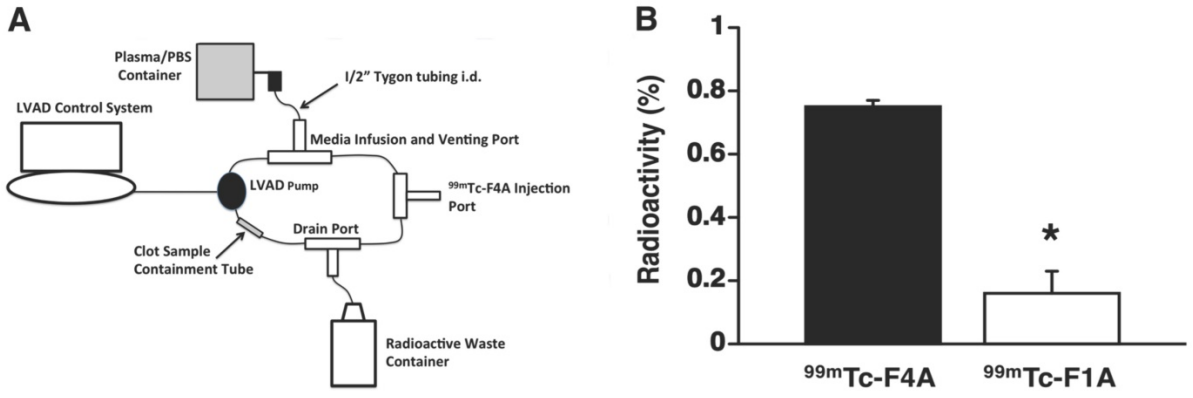

Figure 6. A HMII mock flow loop design: circulation media was 200 mL of heparinized 50:50 plasma:PBS. Activity injected for each probe was 0.5 mCi. **B** Average percent radioactivity (± s.e.m.) of ^{99m}Tc-F4A versus ^{99m}Tc-F1A bound to uniform fibrin clots after 2 min of circulation in HMII mock flow loop. *$p<0.05$, n=3/treatment group, HMII: HeartMate II

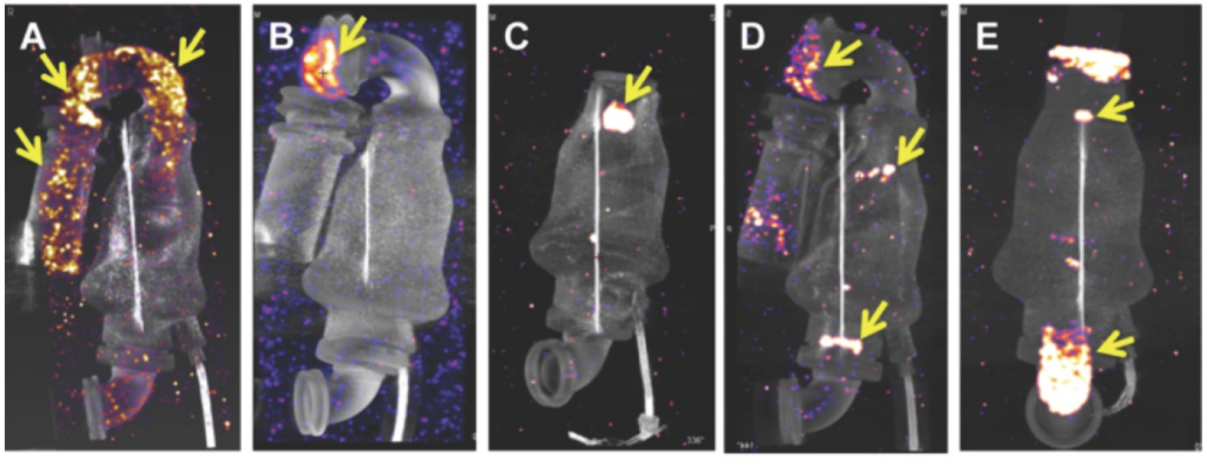

Figure 7. ^{99m}Tc-F4A signal was assessed for the inlet cannula (metallic and Dacron® segments), the inlet stator/bearing, turbine, outlet bearing, and outlet cannula regions. Strong ^{99m}Tc-F4A signals were noted in the metallic and Dacron® inlet cannula segments in **A** and in the flexible, Dacron® segment in panel **B**. Prominent ^{99m}Tc-F4A signal was observed around the inlet bearing in **C** and both the inlet and outlet bearings/stator in **D**. Fibrin accumulation coating the walls of the outlet cannulas were frequently noted as in **E**. This LVAD was notable also for thrombus associated with the inlet and outlet bearings. Yellow arrows in each image point to regions of ^{99m}Tc-F4A signal corresponding to fibrin deposition and accumulation. Abbreviated clinical histories: **A** Implanted 520 days. Early hemolysis after implantation. Peak LDH 1300 U/L. Resolved with eptifibatide and bivalrudin. **B** Implanted 830 days. No hemolysis. Routine transplant. **C** Implanted 146 days. Hemolysis noted with a peak LDH 800 U/L. Negative ramp study. LDH trended downward and the heart was transplanted soon thereafter. **D** Implanted 410 days. Sustained hemolysis with a LDH peak 3400 U/L. Pump exchanged for suspected pump thrombosis. **E** Ischemic stroke 7 days after implantation. No hemolysis. Pump exchanged. LVAD: left ventricular assist device; LDH: lactic dehydrogenase.

Assessments of thrombus in explanted rewired LVADs in a mock loop with ^{99m}Tc-F4A

For further proof of concept of this clot-binding contrast agent, ^{99m}Tc-F4A binding was assessed in explanted LVADs from patients (examples of 5 from over 60 pumps evaluated are shown) receiving heart transplants or surgical pump exchange to demonstrate the imaging agent affinity for the native intra-pump fibrin deposition and to determine if high resolution imaging could spatially characterize the extent of thrombus formation (Figure 7). ^{99m}Tc-F4A signal was assessed for the inlet cannula (metallic and Dacron® graft segments), the inlet stator/bearing, turbine, outlet bearing, and outlet cannula regions. Strong ^{99m}Tc-F4A signals were noted in the metallic and Dacron® inlet cannula segments in Figure 7A and in the flexible, Dacron® segment in Figure 7B. Prominent ^{99m}Tc-F4A signal around the inlet bearing in Figure 7C and both the inlet and outlet bearings/stator in Figure 7D were also observed. Fibrin accumulation coating the walls of the outlet cannulas was frequently noted as in Figure 7E. The occasional LVAD had no detectable ^{99m}Tc-F4A, but the prevalence of HMII pumps with detectable fibrin using a nanoSPECT/CT imaging was high in an initial cohort (17/18). Inherent nonspecific binding of ^{99m}Tc-F4A to the LVAD pump was nondetectable (Figure S1). Additionally, six pumps were submitted to the vendor for independent pathologic evaluation and corroborated the nuclear imaging results (Figure S2).

Discussion

Detection and characterization of LVAD thrombus is an unmet medical need with significant clinical importance in the heart failure community not only for diagnosing pump thrombosis but for better individualizing anticoagulation regimens. ^{99m}Tc-F4A is a prototype tetrameric nuclear probe capable of binding fibrin deposits in the high-shear high-flow chambers within LVADs and is detectable through the titanium pump housings. Four bifunctional monomeric probes (^{99m}Tc-F1A) were connected through a tetrameric polyethylene glycol core to form ^{99m}Tc-F4A. In addition to overcoming high shear, this prototype probe effectively targeted aged thrombus exposed long-term to anticoagulation, which virtually all fibrin-specific contrast agents have failed to target to date [22].

As shown, ^{99m}Tc-F4A had extraordinary binding avidity to fibrin clots that could not be displaced in vitro by the F1A monomeric probe at ratios up to 120,000:1 molar excess. Moreover, in the LVAD ex vivo mock flow loop, the binding affinity of ^{99m}Tc-F1A to fibrin clots was less than ^{99m}Tc-F4A. The bifunctional monomeric ^{99m}Tc-F1A and the tetrameric ^{99m}Tc-F4A share the same cyclic peptide ligand and ^{99m}Tc chelating strategy. While the monomeric probe can associate with a single fibrin fibril, the tetrameric PEG arms allow the ^{99m}Tc-F4A probe to interact with multiple fibrin fibrils or to bind around a single fibril at multiple sites. Hypotheses based on possible 3 dimensional conformations will be complex to resolve but fascinating avenues for future study.

Hydrophobic peptide binding to plasma protein constituents is common among peptide-based probes in general, and was observed for ^{99m}Tc-F1A in the present study as plasma interference with binding in vitro. While the reported specific binding to plasma proteins such as albumin may be low on a micromolar basis, the concentrations of albumin and other plasma proteins in blood are very high (up to 3-4 g/dL). This large capacity of plasma proteins for nonspecific adsorption requires increased probe dosages for targeting purposes and can result in elevated persistent background signal, reducing detection sensitivity for critical small thrombin deposits associated with HMII pump bearings.

Indeed, almost all thrombus probes reported to date bind or accumulate in acute clots, typically less than 72 h, with poorer binding achieved as the thrombus ages and accessible fibrin content decreases. As an example, a recent promising fibrin-binding peptide (FBP8)-PET probe was reported to have efficacy towards acute thrombus, which then diminished quickly as the clot aged. This loss of fibrin binding paralleled a reduction in fibrin content as the clot organized [32, 33]. LVADs presented in this study were obtained from patients 7 to 830 days following implantation. In all instances, the thrombus was an acellular almost pure fibrin accretion. In published reports of severe cases, the intra-pump thrombus deposits had a "woody" layered appearance resembling growth rings in a tree trunk [34].

Anticoagulation with warfarin and aspirin is prescribed chronically to diminish the incidence of thrombosis in LVADs. However, with exception of ^{99m}Tc-NC100668, which employed a partial peptide analogue of alpha$_2$-antiplasmin [35-37], thrombus-specific contrast agents have routinely failed to be effective in the presence of anticoagulation [22]. In the present study, ^{99m}Tc-F4A was effective against aged fibrin deposits in LVADs exposed to anticoagulation during patient use and during ex vivo evaluation in the mock-flow loops.

Given the continued high bleeding and stroke rates associated with LVADs despite close management under current guidelines for anticoagulation management, ^{99m}Tc-F4A may offer a key tool to individualize anticoagulation goals for patients, improving management decisions that minimize GIB and strokes. Although fibrin deposits were noted in the outlet and inlet cannulas and bearings and occasionally along the axial rotor, the clinical relevance of thrombus accumulation in one pump region versus another remains to be fully resolved. LDH is often used as a surrogate clinical marker of pump thrombosis, particularly for very late conditions, but the early correlation between transient spikes in LDH and significant pump thrombosis is uncertain. Similarly, the correlation between LVAD operational voltage variations and spikes alone have not been reliable enough to warrant major clinical decisions, such as pump exchanges, and the relationship between voltage variation and transient pump thrombosis events remains unclear. ^{99m}Tc-F4A is anticipated to provide a robust metric to assess accumulation in LVAD thrombus to help individually tune anticoagulation (INR) targets to minimize stroke and bleeding risk. Periodic testing, particularly in response to clinical status triggers, could be used to affirm or adjust the clinical management plan over time.

^{99m}Tc-F4A was developed with a previously characterized fibrin peptide analogue to test the concept of a tetrameric PEG cross-linked bifunctional probe as a means to overcome the LVAD challenges of aged clot, chronic anticoagulation, and high shear blood flow. While the potential success of this probe is supported by the data presented, chemistry improvements as well as further characterization are required. From a chemistry perspective, ^{99m}Tc-F4A utilized a commercially available tetrameric PEG core with unexpectedly high variability with regard to PEG arm lengths. This variability complicated analytically-supported process scale-up efforts required to conduct additional analytical, in vitro, and in vivo characterization studies. The next generation of probe(s) will require scalable synthesis of the tetrameric PEG including highly controlled individual PEG arm lengths. Additionally, while the present prototype probe was synthesized using solid phase chemistry, the scaled version of ^{99m}Tc-F4A will likely require the adoption of a solution phase method. Improvements in process and characterization will better support large animal LVAD homing studies and improved pharmacokinetic assessments, with high clinical translation relevance.

In summary, ^{99m}Tc-F4A is a prototype probe incorporating a tetrameric PEG core found to achieve high avidity against aged fibrin with minimal plasma matrix interference for direct noninvasive LVAD thrombus assessments. ^{99m}Tc-F4A targeted fibrin effectively in vivo in mice as well as ex vivo in human excised LVADs rewired and operated in a mock-loop. Biodistribution studies demonstrated that the unbound probe cleared rapidly through the urinary system with negligible liver, spleen, or lung accumulation. ^{99m}Tc-F4A detected and spatially characterized thrombus in operational LVADs excised from patients with and without prior suspicion of pump thrombus. ^{99m}Tc-F4A could be applied to investigate biomarkers or clinical symptoms suggestive of pump thrombus formation as well as

better individualize anticoagulation management to minimize bleeding while reducing thrombotic complications and pump exchanges.

Abbreviations

%ID/g: percent injected dose per gram tissue; BD: biodistribution; BT: bridge to transplantation; BW: body weight; Calcd: calculated; CT: computed tomography; Da: daltons; Dmab: 4-{N-[1-(4,4-dimethyl-2,6-dioxocyclohexylidene)-3-methylbutyl]-amino}benzyl; DT: destination therapy; ESI-TOF: electrospray ionization-time of flight mass spectroscopy; F1A: monomeric bifunctional ligand with a fibrin-specific peptide; F4A: tetrameric analogue of F1A; I4A: tetrameric analogue of F1A using an irrelevant homing peptide; GIB: gastrointestinal bleeding; HeNe laser: helium-neon laser; HF: heart failure; HMII: HeartMate II; HPLC: high performance liquid chromatography; INR: International Normalized Ratio; LDH: serum lactic dehydrogenase; LV: left ventricle; LVAD: left ventricular assist device; K_d: dissociation constant; MALDI: Matrix-assisted laser desorption/ionization; MIP: maximum intensity projection; MRI: magnetic resonance imaging; MW: molecular weight; PBS: phosphate buffered saline; PEG: polyethylene glycol; PK: pharmacokinetics; RPM: revolutions per minute; SPECT: single-photon emission counting tomography (SPECT); ^{99m}Tc: technetium-99m.

Acknowledgments

The authors appreciate and recognize the kind contributions of Douglas M. Tollefsen, M.D., Ph.D. who helped establish the carotid thrombosis model using laser excited Rose Bengal dye.

Financial support: Partial funding support was received from the Barnes-Jewish Hospital Research Foundation, St Louis, MO, 63110 and from the NIH: HL122471, HHSN268201400042C, HL112518, HHSN268201400042C, HL112518, HL113392, CA199092, CA154737.

Supplementary Material

Supplementary figures and methods.
http://www.thno.org/v08p1168s1.pdf

Competing Interests

Washington University (GC, SA, GL) has filed for intellectual property rights related to technology described in this manuscript. Capella Imaging, LLC (GC, GL) was recently founded to translate this technology to patients. The remaining authors have nothing to disclose. Abbott-Thoratec provided an LVAD computer controller to support the ex vivo mock loop studies and provided independent assessments of LVAD thrombus consistent with a global device inspection protocol for returned pumps from any institution.

References

1. Go AS, Mozaffarian D, Roger VL, Benjamin EJ, Berry JD, Blaha MJ, et al. Heart disease and stroke statistics-2014 update: a report from the American Heart Association. Circulation. 2014; 129: e28-e292.
2. Yancy CW, Jessup M, Bozkurt B, Butler J, Casey DE, Jr., Drazner MH, et al. 2013 ACCF/AHA guideline for the management of heart failure: a report of the American College of Cardiology Foundation/American Heart Association Task Force on Practice Guidelines. J Am Coll Cardiol. 2013; 62: e147-239.
3. Taylor DO, Stehlik J, Edwards LB, Aurora P, Christie JD, Dobbels F, et al. Registry of the International Society for Heart and Lung Transplantation: Twenty-sixth official adult heart transplant report-2009. J Heart Lung Transplant. 2009; 28: 1007-22.
4. Rogers JG, Boyle AJ, O'Connell JB, Horstmanshof DA, Haas DC, Slaughter MS, et al. Risk assessment and comparative effectiveness of left ventricular assist device and medical management in ambulatory heart failure patients: design and rationale of the ROADMAP clinical trial. Am Heart J. 2015; 169: 205-10 e20.
5. Estep JD, Starling RC, Horstmanshof DA, Milano CA, Selzman CH, Shah KB, et al. Risk assessment and comparative effectiveness of left ventricular assist device and medical management in ambulatory heart failure patients: results from the ROADMAP study. J Am Coll Cardiol. 2015; 66: 1747-61.
6. Crow S, Chen D, Milano C, Thomas W, Joyce L, Piacentino V, 3rd, et al. Acquired von Willebrand syndrome in continuous-flow ventricular assist device recipients. Ann Thorac Surg. 2010; 90: 1263-9.
7. Yuan N, Arnaoutakis GJ, George TJ, Allen JG, Ju DG, Schaffer JM, et al. The spectrum of complications following left ventricular assist device placement. J Card Surg. 2012; 27: 630-8.
8. Hasin T, Marmor Y, Kremers W, Topilsky Y, Severson CJ, Schirger JA, et al. Readmissions after implantation of axial flow left ventricular assist device. J Am Coll Cardiol. 2013; 61: 153-63.
9. Kapur NK, Vest AR, Cook J, Kiernan MS. Pump thrombosis: a limitation of contemporary left ventricular assist devices. Curr Probl Cardiol. 2015; 40: 511-40.
10. Nassif ME, LaRue SJ, Raymer DS, Novak E, Vader JM, Ewald GA, et al. Relationship between anticoagulation intensity and thrombotic or bleeding outcomes among outpatients with continuous-flow left ventricular assist devices. Circ Heart Fail. 2016; 9: e002680.
11. Kantorovich A, Fink JM, Militello MA, Bauer SR, Soltesz EG, Moazami N. Comparison of anticoagulation strategies after left ventricular assist device implantation. ASAIO J. 2016; 62: 123-7.
12. Slaughter MS, Naka Y, John R, Boyle A, Conte JV, Russell SD, et al. Post-operative heparin may not be required for transitioning patients with a HeartMate II left ventricular assist system to long-term warfarin therapy. J Heart Lung Transplant. 2010; 29: 616-24.
13. Starling RC, Moazami N, Silvestry SC, Ewald G, Rogers JG, Milano CA, et al. Unexpected abrupt increase in left ventricular assist device thrombosis. N Engl J Med. 2014; 370: 33-40.
14. Stulak J, Lee D, Haft J, Romano M, Cowger J, Park S, et al. Gastrointestinal bleeding and subsequent risk of thromboembolic events during support with a left ventricular assist device. J Heart Lung Transplant. 2014; 33: 60-4.
15. Mehra MR, Stewart GC, Uber PA. The vexing problem of thrombosis in long-term mechanical circulatory support. J Heart Lung Transplant. 2014; 33: 1-11.
16. Kirklin JK, Naftel DC, Kormos RL, Pagani FD, Myers SL, Stevenson LW, et al. Interagency registry for Mechanically Assisted Circulatory Support (INTERMACS) analysis of pump thrombosis in the HeartMate II left ventricular assist device. J Heart Lung Transplant. 2014; 33: 12-22.
17. Najjar SS, Slaughter MS, Pagani FD, Starling RC, McGee EC, Eckman P, et al. An analysis of pump thrombus events in patients in the HeartWare ADVANCE bridge to transplant and continued access protocol trial. J Heart Lung Transplant. 2014; 33: 23-34.
18. Cowger JA, Romano MA, Shah P, Shah N, Mehta V, Haft JW, et al. Hemolysis: a harbinger of adverse outcome after left ventricular assist device implant. J Heart Lung Transplant. 2014; 33: 35-43.
19. Shah S, Mehra MR, Couper GS, Desai AS. Continuous flow left ventricular assist device related aortic root thrombosis complicated by left main coronary artery occlusion. J Heart Lung Transplant. 2014; 33: 119-20.
20. Uriel N, Morrison KA, Garan AR, Kato TS, Yuzefpolskaya M, Latif F, et al. Development of a novel echocardiography ramp test for speed optimization and diagnosis of device thrombosis in continuous-flow left ventricular assist devices: the Columbia ramp study. J Am Coll Cardiol. 2012; 60: 1764-75.
21. Krishnan B, Yarmohammadi H, Eckman P, Adatya S. Outflow thrombus in a left ventricular-assist device: visualization by CT angiography. J Cardiovasc Comput Tomogr. 2014; 8: 473-4.
22. Lanza G, Cui G, Schmieder A, Zhang H, Allen J, Scott M, et al. An unmet clinical need: The history of thrombus imaging. J Nucl Cardiol 2017; DOI 10.1007/s12350-017-0942-8.

23. Prasad S, Robertson J, Itoh A, Joseph S, Silvestry S. Histologic analysis of clots in explanted axial continuous-flow left ventricular assist devices. J Heart Lung Transplant. 2015; 34: 616-8.
24. Meyer AL, Malehsa D, Budde U, Bara C, Haverich A, Strueber M. Acquired von Willebrand syndrome in patients with a centrifugal or axial continuous flow left ventricular assist device. JACC Heart failure. 2014; 2: 141-5.
25. Adatya S, Bennett MK. Anticoagulation management in mechanical circulatory support. J Thorac Dis. 2015; 7: 2129-38.
26. Kolodziej AF, Nair SA, Graham P, McMurry TJ, Ladner RC, Wescott C, et al. Fibrin specific peptides derived by phage display: characterization of peptides and conjugates for imaging. Bioconjug Chem. 2012; 23: 548-56.
27. Albericio F. Solid-Phase Synthesis: A Practical Guide. Boca Raton, FL: CRC Press; 2000.
28. Waibel R, Alberto R, Willuda J, Finnern R, Schibli R, Stichelberger A, et al. Stable one-step technetium-99m labeling of His-tagged recombinant proteins with a novel Tc(I)-carbonyl complex. Nat Biotechnol. 1999; 17: 897-901.
29. Bigott-Hennkens HM, Dannoon SF, Noll SM, Ruthengael VC, Jurisson SS, Lewis MR. Labeling, stability and biodistribution studies of ^{99m}Tc-cyclized Tyr3-octreotate derivatives. Nucl Med Biol. 2011; 38: 549-55.
30. Westrick RJ, Winn ME, Eitzman DT. Murine models of vascular thrombosis (Eitzman series). Arterioscler Thromb Vasc Biol. 2007; 27: 2079-93.
31. Vicente CP, He L, Pavao MS, Tollefsen DM. Antithrombotic activity of dermatan sulfate in heparin cofactor II-deficient mice. Blood. 2004; 104: 3965-70.
32. Blasi F, Oliveira BL, Rietz TA, Rotile NJ, Day H, Naha PC, et al. Radiation dosimetry of the fibrin-binding probe ^{64}Cu-FBP8 and Its feasibility for PET imaging of deep vein thrombosis and pulmonary embolism in rats. J Nucl Med. 2015; 56: 1088-93.
33. Blasi F, Oliveira BL, Rietz TA, Rotile NJ, Naha PC, Cormode DP, et al. Multisite thrombus imaging and fibrin content estimation with a single whole-body PET scan in rats. Arterioscler Thromb Vasc Biol. 2015; 35: 2114-21.
34. Prasad. SM, Robertson. JO, Itoh. A, Joseph. SM, Silvestry. SC. Histologic analysis of clots in explanted axial continuous-flow left ventricular assist devices. J Heart Lung Transplant. 2015; 34: 616-8.
35. Edwards D, Lewis J, Battle M, Lear R, Farrar G, Barnett DJ, et al. ^{99m}Tc-NC100668, a new tracer for imaging venous thromboemboli: pre-clinical biodistribution and incorporation into plasma clots in vivo and in vitro. Eur J Nucl Med Mol Imaging. 2006; 33: 1258-65.
36. Edwards D, Lewis J, Battle M, Lear R, Farrar G, Barnett DJ, et al. The biodistribution of NC100668 and the effect of excess NC100668 on the biodistribution and kidney retention of ^{99m}Tc-NC100668 in the rat. Nucl Med Biol. 2007; 34: 315-23.
37. Edwards D, Lewis J, Battle M, Lear R, Farrar G, Jon Barnett D, et al. ^{99m}Tc-NC100668, an agent for imaging venous thromboembolism: The effect of anticoagulant or thrombolytic therapy on the uptake and retention of radioactivity in blood clots in vivo. Nucl Med Commun. 2007; 28: 55-62.